Journal of Hazardous Materials 405 (2021) 123999

Contents lists available at ScienceDirect

Journal of Hazardous Materials

journal homepage: www.elsevier.com/locate/jhazmat

Applicability of TiO_2(B) nanosheets@hydrochar composites for adsorption of tetracycline (TC) from contaminated water

Zhu Mengting [a,1], Tonni Agustiono Kurniawan [a,b,*,1], Ram Avtar [c,**], Mohd Hafiz Dzarfan Othman [d], Tong Ouyang [a], Huang Yujia [a], Zhang Xueting [a], Tjandra Setiadi [e], Iswanto Iswanto [f]

[a] Key Laboratory of the Coastal and Wetland Ecosystems (Xiamen University), Ministry of Education, College of the Environment and Ecology, Xiamen University, Fujian 361102, China
[b] Department of Energy, Environment, and Climate Change, School of Environment Resources and Development (SERD), Asian Institute of Technology (AIT), Pathumthani 12120, Thailand
[c] Faculty of Environmental Earth Sciences, Hokkaido University, Sapporo 060-0810, Japan
[d] Advanced Membrane Technology Research Centre (AMTEC), School of Chemical and Energy Engineering, University Teknologi Malaysia, 81310 Skudai, Johor, Malaysia
[e] Center for Environment Studies, Bandung Institute of Technology (ITB), Bandung 40135, Indonesia
[f] Poltekkes, Kemenkes, Yogyakarta 55293, Indonesia

ARTICLE INFO

Keywords:
Antibiotics
Adsorption
H-bond
Low-cost adsorbent
Refractory pollutant

ABSTRACT

We test the feasibility of TiO_2(B)@carbon composites as adsorbents, derived from wheat straws, for tetracycline (TC) adsorption from aqueous solutions. Hydrochar (HC), biochar (BC), and hydrochar-derived pyrolysis char (HDPC) are synthesized hydrothermally from the waste and then functionalized with TiO_2(B), named as 'Composite-1′, 'Composite-2′, and 'Composite-3′, respectively. A higher loading of TiO_2(B) into the HC was also synthesized for comparison, named as 'Composite-4′. To compare their physico-chemical changes before and after surface modification, the composites are characterized using FESEM-EDS, XRD, BET, FRTEM, and FTIR. The effects of H_2O_2 addition on TC removal are investigated. Adsorption kinetics and isotherms of TC removal are studied, while TC adsorption mechanisms are elaborated. We found that the Composite-4 has the highest TC removal (93%) at pH 7, 1 g/L of dose, and 4 h of reaction time at 50 mg/L of TC after adding H_2O_2 (10 mM). The TC adsorption capacities of the Composite-1 and Composite-4 are 40.65 and 49.26 mg/g, respectively. The TC removal by the Composite-1 follows the pseudo-second order. Overall, this suggests that converting the wheat straw into HC and then functionalizing its surface with TiO_2(B) as a composite has added values to the waste as an adsorbent for wastewater treatment.

1. Introduction

In recent years, water contaminations by antibiotics, excreted from humans and animals in the water body and soil matrix, have emerged as one of the most important environmental issues worldwide (Zhang et al., 2015). Among the antibiotics, tetracycline (TC), widely used in human and veterinary medicines, is frequently detected in local wastewater treatment plants (WWTPs). Its trace concentrations in surface water range from 0.01 to 20 μg/L (Liu et al., 2018). After preliminary treatment using low-cost biological processes, the pollutant is still present in the WWTPs. As a result, there is growing public concern due to its long-term impacts on aquatic organisms and public health, as biological process alone is not effective to deal with refractory contaminants in the water body.

Over the past years, physico-chemical techniques such as oxidation (Kurniawan et al., 2006a; 2006b), membrane bioreactor (Chan et al., 2007), and photodegradation (Zhu et al., 2019) have been tested for water treatment applications. Compared to those treatments, recently

* Corresponding author at: Key Laboratory of the Coastal and Wetland Ecosystems (Xiamen University), Ministry of Education, College of the Environment and Ecology, Xiamen University, Fujian 361102, China.
** Corresponding author.
E-mail addresses: tonni@xmu.edu.cn (T.A. Kurniawan), ram@ees.hokudai.jp (R. Avtar).
[1] The first and second authors equally contributed to this article and mutually share the first authorship.

https://doi.org/10.1016/j.jhazmat.2020.123999
Received 9 December 2019; Received in revised form 12 September 2020; Accepted 14 September 2020
Available online 17 September 2020

adsorption using low-cost materials has attracted popularity due to its simple and convenient operations, low energy consumption, and technical applicability (Babel and Kurniawan, 2003; 2004).

With respect to the circular economy and cleaner production paradigms (Kurniawan et al., 2013), recently we have searched for non-conventional materials from biomass. As a natural source of green energy, it generates a variety of by-products that need to be further recycled and reused in order to close the loop of circular economy.

Wheat straw, a part of stem and leaf that remains after the wheat ripens, is an agricultural waste from a local industry in China. Due to its high disposal cost, a large quantity of the waste is improperly disposed of in local landfills without considering its recycling value. Such unused resources, which represent raw materials for wheat straw waste-derived carbon materials including hydrochar (HC), biochar (BC), and hydrochar-derived pyrolysis char (HDPC), have emerged as one of the most promising options due to their polar affinity toward certain aquatic contaminants caused by the delocalized furanic conjugated system (Kearns et al., 2014).

To enhance its removal performance, surface modification of BC with other functional materials in the form of a composite that may be utilized as a low-cost adsorbent for water treatment would add its economic value and decrease waste disposal cost, providing an option to costly activated carbon for restoring contaminated water body (Kurniawan et al., 2010a, 2011). The exchange properties of the waste are attributed to the presence of functional groups, such as carboxyl, carbonyl, hydroxyl, and heterocyclic carbons, which have a high affinity for hydrophilic compounds (Li et al., 2013).

Biochar (BC) is rich in carbon. This material results from hydrothermal carbonization at 250 °C of temperature (Lehmann and Joseph, 2015), while hydrochar (HC) is an industrial by-product, resulting from a hydrothermal carbonization of C-rich biomass (Xue et al., 2012). Unlike the BC, the hydrothermal process of the HC is eco-friendly and does not transfer any hazardous pollutants into the environment. By utilizing biochar for environmental applications, about one-eighth of greenhouse gases (GHG) emissions, resulting from human activities, could be decreased (Woolf et al., 2010).

In addition, Ahmad et al. (2014) and Meyer et al. (2011) found that the production cost of BC was only less than 2% of that of activated carbon. Considering its attractive cost, developing low-cost adsorbents such as BC is necessary to remediate the aquatic environment cost-effectively. Currently the global market size of BC was about US$ 1.3 billion in 2013, while its demand was approximately about 0.4 megatonne (Mt) (Narzari et al., 2014).

In a recent study, Han et al. (2017) reported that corncob waste-derived HDPC exhibited three times higher adsorption capacity (138 mg/g) for butanol than did HC (66 mg/g). Without any surface modification, raw carbon materials (HC, BC, and HDPC) have a low TC removal (Zhu et al., 2013). To improve their removal for TC, the carbon materials need to be functionalized with other materials such as TiO_2(B) nanosheets in the form of composite to enable them to have novel and complementary physico-chemical properties useful and appropriate for water treatment applications. It is expected that the composite would have distinct advantages toward target pollutant with respect to selectivity or capacity (Kurniawan et al., 2006c, 2006d).

The TiO_2(B) is a monoclinic allotrope of TiO_2 that has the lowest density (Kommireddy et al., 2006). The TiO_2(B) had a higher TC removal than did the pure TiO_2, as it had a large surface area that could act as an effective catalyst (Kurniawan et al., 2020; Zhu et al., 2020a). Unlike TiO_2(B) pristine nanosheet, the TiO_2(B)@carbon materials have distinct advantages for water treatment applications such as low cost, non-toxicity, large surface area, and good reactivity (Fu et al., 2017).

According to Yao et al. (2017) and Nadeem et al. (2018), TiO_2(B) nanosheet has unique surfaces in its interface with water. When bridging hydroxyls happens due to water dissociation in oxygen vacancies between O_{2c} and Ti_{5c} atoms, there are physico-chemical interactions between the carbonyl functional group of the TC with the Ti_{5c} and the O_{2c} atom of the TiO_2(B) nanosheet in its surface. This interaction that contributes to the formation of H-bonding for TC removal occurs through electrons transfer via *Ti–O–C* bond (through the oxygen atom) from the TiO_2(B) nanosheet to the carbonyl group of the TC. Both Ti_{5c} and O_{2c} represent to the surface five-fold coordinated Ti and two-fold coordinated O of the TiO_2(B) nanosheet, respectively.

In spite of its attractive performance for water treatment, to the best of our knowledge, no one has so far reported tangible changes in the physico-chemical properties of the TiO_2(B) nanosheet@carbon composites due to the effects of H_2O_2 incorporated into the reaction system in terms of TC removal by the composites. The addition of H_2O_2 in the adsorption reaction was to promote oxidative reactions between target pollutant and the reactive TiO_2(B)@carbon materials so that the TC could be removed simultaneously through both oxidation and adsorption process (Kurniawan and Lo, 2009).

With respect to its novelty, we uncovered the technological values and potential of unused wheat straw waste as an adsorbent – after being functionalized with the TiO_2(B) nanosheet – that can be used for water treatment applications. Hence, this work provides both engineering and scientific perspectives, while offering rational for the applications of the composites, derived from non-conventional resources, for water treatment purposes (Lin et al., 2017, 2018a).

In this study, we investigated the applicability of the TiO_2(B)@carbon materials (HC, BC, and HDPC) composites, derived from the wheat straw waste, as a potential adsorbent for removal of TC from aqueous solutions using adsorption process. After their synthesis, the properties of the composites were characterized using XRD, an elemental analyzer, FTIR, FESEM-EDS, BET and HRTEM. The effects of additional H_2O_2 on the physico-chemical properties of the composites for TC removal were investigated, while the removal pathways of the TC by the composites are elaborated.

2. Materials and methods

2.1. Materials

Tetracycline (98%) (Fig. S1) was obtained from Aladdin Industrial Corporation (Shanghai, China), while other chemicals such as NaOH, HCl, $TiCl_4$, ethylene glycol (EG), H_2O_2 (30% (w/w)) were supplied by Sinopharm Chemical (China). The chemicals we used in this study were of analytical grade. The TC working solutions were freshly prepared before their use.

2.2. Synthesis of composites

Anaerobically digested wheat straw waste was obtained from a biogas plant at the Nanjing Technology University (China) after three months of anaerobic fermentation. The waste was processed at the plant at 328 K for 2 h. The waste was subsequently dewatered and dried in an oven at 383 K for 2 d. Afterward, the size of their particles was reduced using a mill to 0.15 mm of sieve for their uniformity.

The synthesis techniques of HC, BC, and HDPC, derived from the wheat straw waste, were reported earlier by Garlapalli et al. (2016). Initially, the HC was produced by using 10 g of the waste and 80 mL of ultrapure water to maintain a constant biomass-to-water-ratio of 1:8. Subsequently, the mixture was transferred into a stainless steel reactor. After heating the mixture to 453 K for 6 h and subsequent cooling for 12 h, the product was filtered, washed with ultrapure water, and dried at 383 K for 2 d. For BC and HDPC, 10 g of the waste and/or its HC were carbonized in a tubular furnace at 773 K for 2 h at 400 mL/min of N_2 flow.

To functionalize the surface of HC, BC, and/or HDPC, respectively, with the TiO_2(B) nanosheet, their composites were synthesized based on a sol-gel method (Lisowski et al., 2017). One gram of the HC was immersed into a mixture containing 30 mL of EG, 0.4 mL of $TiCl_4$, and 1 mL of water (Table S1). Afterward, the mixture was sonicated for 1 h and

it was transferred into a 100 mL non-stirred T316 stainless steel reactor. The hydrothermal conditions were set at 423 K for 6 h. After cooling for 12 h, the mixture was filtered, repeatedly washed by ultrapure water, and then dried in an oven at 383 K. The resulting products were referred as 'Composite-1′. The flowchart of the synthesis process is illustrated in Fig. S2, while the mass proportion of TiO_2 in each composite is listed in Table S1.

For comparison, both the Composite-2 and the Composite-3 were also synthesized using the same sol-gel method, as presented in Table S1. A higher loading of the TiO_2(B) nanosheet into the HC with the addition of 1.0 mL of $TiCl_4$ and 1 g of the HC was also synthesized, named as 'Composite-4′.

2.3. Characterization of adsorbents

The composition of C, H, N, and S in carbon materials and/or in their composites was determined using an elemental analyzer (model Vario MICRO Cube, Germany). Their crystallinity was analyzed using an X-ray diffractometer (XRD, Rigaku, Japan) using Cu Kα radiation, which operated at 40 kV and 30 mA at 10°/min. The BET (Brunauer–Emmett–Teller) specific surface areas of the samples were tested using an N_2 adsorption−desorption isotherm analysis carried out at 77 K (model ASAP 2020, US). Their FT−IR (Fourier transform infrared) spectra were also recorded on an IS50 FT−IR (type Thermo, USA) in the range of 4000–400 cm^{-1} with a resolution of 0.2 cm^{-1}. To analyze changes in their morphologies before and after surface modification, tests using a field emission scanning electron microscopy coupled with energy dispersive spectroscopy (FESEM-EDS, model Sigma, SEISS, Germany) were conducted. The inner structure of the film was determined by using a high-resolution transmission electron microscopy (HRTEM type Tecnai F30, the Netherlands).

2.4. Batch studies

2.4.1. Adsorption reaction

To determine the most effective carbon materials (either HC, BC or HDPC) and their composites (after being functionalized with the TiO_2(B) nanosheet), TC adsorption tests were conducted in batch reactors. About 0.02 g of the adsorbent was mixed with 20 mL of synthetic wastewater with 50 mg/L of TC. The reactors were agitated on a rotary shaker (model ZQTY-50S, Shanghai, China) under optimum conditions. To avoid undesirable interference with TiO_2 by UV–vis, the experiments were carried out in darkness (Yusof et al., 2020a). If TiO_2(B) nanosheets were used under UV–vis irradiation, it would result in photocatalytic response due to the narrowing bandgap and increasing active sites of the TiO_2(B) nanosheet (Kong et al., 2018; Kurniawan et al., 2018).

2.4.2. Adsorption kinetics and isotherms

The kinetics and isotherm studies of the HC and its composites (Composite-1 and Composite-4) were conducted at ambient temperature based on the study undertaken by Fu et al. (2017). Initially, the TC batch studies were carried out at 298 K. Afterward, 0.02 g of the adsorbent was added into 20 mL of synthetic wastewater with a predetermined TC concentration at pH 5.8. Its adsorption kinetics were investigated by using 10 mg/L of TC with varying reaction time from 10 to 240 min, while the isotherms studies were performed by varying TC concentrations from 5 to 100 mg/L. The samples were collected periodically using syringes and filtered through 0.22 μm membrane for chemical analyses, while the saturated composites after treatment were collected for regeneration.

Their kinetics data were fitted by the pseudo-first-order (Eq. (1)), pseudo-second-order (Eq. (2)) and intra-particle diffusion (Eq. (3)) models, respectively, as reported earlier by Yusof et al. (2020a, 2020b) as follows:

$$q_t = q_e\left(1 - e^{-k_1 t}\right) \tag{1}$$

$$q_t = \frac{k_2 q_e^2 t}{1 + k_2 q_e t} \tag{2}$$

$$q_t = k_i t^{0.5} \tag{3}$$

where q_t (mg/g) and q_e (mg/g) represent the adsorbed amount of TC at time t (min) and at equilibrium, respectively; k_1 (min^{-1}) is the pseudo-first-order constant and k_2 (g/mg·min) is the initial adsorption rate, respectively; while k_i (mg/g·$min^{1/2}$) is the intraparticle diffusion rate constant.

Their adsorption isotherms data were simulated using the Langmuir and the Freundlich models, respectively, as reported by Mangwandi et al. (2020) as follows:

$$q_t = \frac{k_L q_m C_e}{1 + k_L C_e} \tag{4}$$

$$q_t = k_F C_e^{1/n} \tag{5}$$

where q_m (mg/g) is the maximum adsorption capacity, while k_L (L/mg) and k_F ($mg^{(1-n)}$ L^n/g) represent the Langmuir constants and the Freundlich equilibrium concentration of the adsorbate, respectively; while n is the Freundlich linearity constant.

2.4.3. Effects of H_2O_2 addition on TC removal by the composites

The effects of additional H_2O_2 on TC removal by the Composite-1 and/or the Composite-4 during the reaction were studied using the oxidant's varying concentrations from 1 to 20 mM. The initial concentration of TC used was 10 mg/L. To prevent undesirable interference of UV-vis on the oxidant and /or TiO_2(B) of the Composites, the experiments were conducted in darkness. To prevent the H_2O_2 from releasing active species involved in TC degradation, control experiments with H_2O_2 alone in the absence of the TiO_2(B)@HC were carried out based on Chen et al. (2017a).

2.4.4. Regeneration

After treatment, the spent adsorbent containing adsorbed TC was collected for regeneration. The saturated Composite-1 was repeatedly washed with ultrapure water to remove any unadsorbed TC. Desorption was carried out by soaking the exhausted adsorbent with 100 mL of 0.1 M NaOH. The same sample was then washed with ultrapure water until its pH ranged between 7.0 and 7.2. The regenerated Composite-1 was reused for the consecutive cycles of TC adsorption. Their regeneration efficiencies (%) were determined based on the study undertaken by Lin et al. (2017) as follows:

$$(\%RE) = \left(\frac{A_r}{A_0}\right) \times 100\% \tag{6}$$

where A_o and A_r are the adsorption capacities of virgin and regenerated composite (mg/g), respectively.

2.5. Chemical analyses of TC

The remaining TC concentrations after the adsorption treatment were determined by a UV–vis spectrophotometer (model UV-1700, Shimadzu, Japan) at 360 nm of wavelength (λ_{max}). The equilibrium adsorption uptake, q_e (mg/g) and removal efficiency (η(%)) of TC were calculated according to the study carried out by Fu et al. (2017) as follows:

$$q_e = \left(\frac{C_0 - C_t}{w}\right) V \tag{7}$$

$$\eta(\%) = \left(\frac{C_0 - C_t}{C_0}\right) \times 100\% \tag{8}$$

where q_e is the TC adsorption capacity (mg/g), C_0 and C_e are the initial and final TC concentrations (mg/L), respectively, while V is the volume of solution (L) and w is the dry weight of the adsorbent (g).

2.6. Statistical analysis

These batch experiments were undertaken using the same method in triplicate under identical conditions to ensure data reproducibility. The obtained data were statistically tested using SPSS 25.0 Version with $p \leq 0.05$ indicating significant differences.

3. Results and discussion

3.1. Characterization of adsorbents

3.1.1. BET analysis

Prior to adsorption studies, the wheat straw waste-derived carbon materials and their composites were tested for carbonization, which refers to the conversion of wheat straw waste to carbon materials. The properties of the adsorbents after carbonization are presented in Table S2. The table shows that the yields of the carbon materials ranged from 35 to 67%. The low carbon content in the adsorbents (HC, BC, and HDPC) was due to their anaerobic digestion, where they were converted into methane.

The specific surface areas (S_{BET}) of all of the samples are also listed in Table S2. As compared to the raw carbon materials (HC, BC, or HDPC), the S_{BET} of Composites 1–4 significantly increased, respectively, after being functionalized with the TiO_2(B) nanosheet on their surface. The initial BET surface area of HC was 21 m^2/g, but after being present in the form of the Composite-4, its surface area substantially increased by 805% (up to 190 m^2/g) (Table S2). This could be due to the enhanced pore volume of the Composite-4 by 128% from 0.14 to 0.32 cm^3/g (Albadarin et al., 2017).

This encouraging result was in agreement with the findings reported earlier by Gerasimova et al. (2016), who reported that the increasing BET surface was partly due to the increasing pore volume of the Composite. It was also found that the pore size of the Composite-4 decreased by 76% from 28.2 to 6.7 nm, suggesting that the adsorption capacity of the Composite-4 improved (Kumar et al., 2019).

3.1.2. FESEM–EDS and TEM analyses

The morphological and elemental distribution of the four composites used in this study were characterized using a FESEM-EDS (Fig. 1). Distinct and rough particles were observed in the Composite-2 and the Composite-3, respectively. On the other hand, the Composite-1 exhibited a relatively dense and fine surface. The EDS analysis of the Composite-1 presented the existence of C, O and Ti elemental compositions, indicating the co-existence of the HC and TiO_2(B) nanosheet as a composite. Although both the HC and TiO_2(B) were attached to each other via the *Ti–O–C* bond, the pulverization and aggregation of the TiO_2(B) nanosheets might be able to hinder the surface of the carbon materials from being coated, as reported by Chen et al. (2017b).

The HRTEM results, presented in Fig. S3(a–c), demonstrated obvious differences in terms of morphology between the TiO_2(B) alone and the TiO_2(B)@HC (Composite-1). It was clear from the dark area that the TiO_2(B) existed in nanosheet form (Fig. S3a), while the Fig. S3b represents the porous structure of the HC. Although there are variations of growth mechanisms at atomic scale for the Composite-1, Fig. S3(c) depicts that the TiO_2(B) was anchored physically on the surface of the HC after being hybridized.

Even though both the starting materials have different physical properties, it is difficult to visually distinguish the carbon material from the TiO_2(B) in Fig. S3c after forming the Composite-1, because the surface of HC is densely packed with the TiO_2(B) nanosheets via the *Ti–*

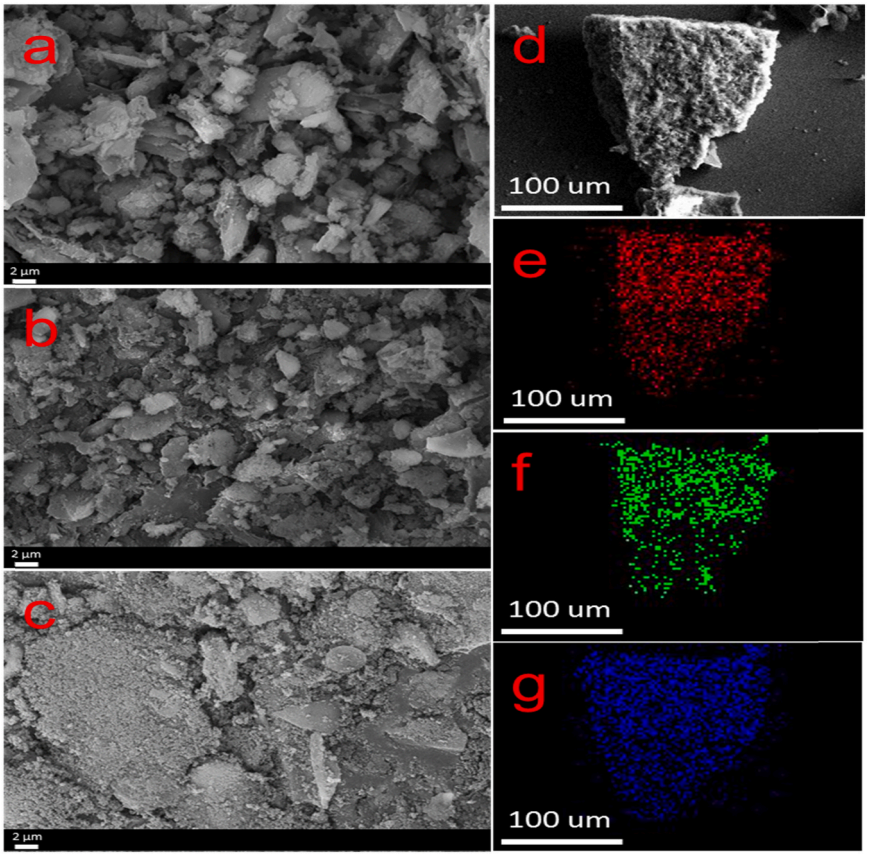

Fig. 1. FESEM images of Composite-2 (a), Composite-3 (b), and Composite-1 (c and d) and EDS elemental mappings of Composite-1 (C (e), O (f), and Ti (g)).

O–C bond and the resulting Composite-1 is visualized at atomic scale. The same Fig. S3(c), which presents agglomerated particles on the surface of the Composite-1, is obviously different from the Fig. S3(a) due to co-existence of both the TiO_2(B) and the surface of the HC. This result was consistent with the findings reported by Xiang et al. (2010), who observed the same nanosheets structure that was incorporated on the surface of the TiO_2(B)@HC (Composite-1) (Fig. S3c).

It was evident that the sol-gel method facilitated the formation of the TiO_2(B) on the surface of the HC (Fig. S3b) during hybridization. Other characterization data from the XRD and FTIR tests also supported and verified the formation of the TiO_2(B)@HC (Composite-1), apart from those obtained from the FESEM and the EDS. Overall, these characterization data have obviously indicated the co-existence of the TiO_2(B) and the HC in the form of 'Composite-1'.

3.1.3. XRD and FTIR analyses

The crystallinity of the TiO_2(B) nanosheet was also analyzed using XRD tests. In spite of the lower loading amount of the TiO_2(B) into the HC (Table S1), the Composites-1 exhibited strong characteristic peaks of the TiO_2(B) (Fig. 3), as indicated by the diffraction peaks (1 1 0), (0 0 2), and (0 2 0). Those peaks can be well assigned to the TiO_2(B) (JCPDS No. 74–1940). The increasing peak strength of the Composite-1 at 7.5° suggests that the coated TiO_2(B) possessed an interlayer structure of the 2D morphology. The two sharp peaks of the TiO_2(B)@HC and the HC at $2\theta = 25.4°$ (Fig. 2) represent the characteristic peaks of the HC, which were consistent with the results reported by Donar et al. (2018). The amorphous structure of the carbon in the cellulose caused the diffraction peaks broaden because the HC was predominantly composed of cellulose (Donar et al., 2018).

The FTIR analyses of the HC, TiO_2(B), and the Composite-1 are presented in Fig. 3. As compared to the HC and the TiO_2(B), the Composite-1 exhibited unique peaks of the TiO_2(B) and other corresponding peaks at 2872 cm^{-1} and 2936 cm^{-1}, at 1630 cm^{-1}, and 1117 cm^{-1}, which indicated the formation of $–CH_2–$, –OH, and C–O groups, respectively. The results suggest that their formation was attributed to the EG solvent, which was used during the functionalization of HC with the TiO_2(B).

3.2. Adsorption studies

3.2.1. TC removal by different composites

As depicted in Fig. 4, after 4 h of reaction, the Composite-4 exhibited the highest TC removal (65.5%) with an initial TC concentration of 50 mg/L. Although the Composite-4 had a higher TC removal than did the Composite-1 due to its higher loading amount of TiO_2 (Table S1), both the composites had a reasonable TC removal. In this process adsorption alone plays key roles in TC removal from aqueous solutions

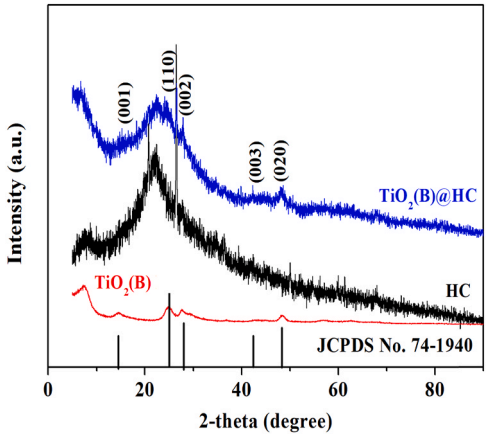

Fig. 2. XRD analyses of TiO_2(B), HC, and (b) Composite-1.

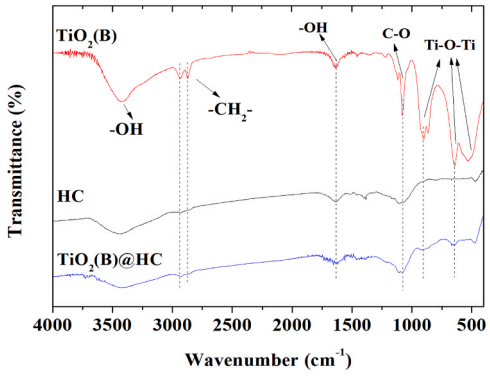

Fig. 3. FTIR analyses of pristine TiO_2(B), HC, and Composite-1.

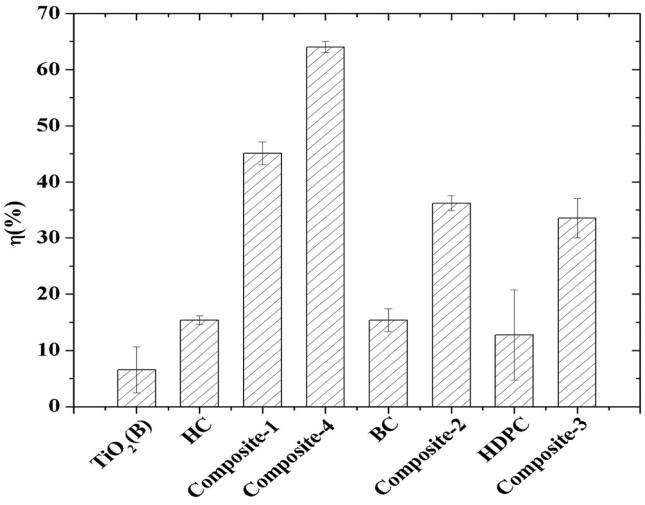

Fig. 4. Removal of TC by carbon materials before and after impregnation with TiO_2(B). (Conditions: pH: 7; 1 g/L of dose, reaction time: 4 h; TC concentration: 50 mg/L).

by the TiO_2(B)−functionalized composite. Principally, it is a process of mass transfer by which an adsorbate is transferred from the aqueous phase to the surface of a solid, and then bound by physico-chemical forces (Kurniawan et al., 2006c; 2006d).

This finding was in agreement with that reported by Kambo and Dutta (2015), who also found that the HC had a higher adsorption capability for TC than did other carbon materials due to the presence of rich oxygen-containing functional groups on its surface. It is important to note that the high removal of TC by the composite was attributed neither to the TiO_2(B) nanosheet nor to the carbon materials, derived from the wheat straw waste.

Fig. 4 also shows that the sole TiO_2(B) nanosheet had the lowest TC removal, while all of the Composites had a relatively higher TC removal, as compared to their starting carbon materials (HC, BC and HDPC) and the TiO_2(B) nanosheet alone. On the other hand, the high removal of TC by the Composite-4 was due to the synergistic effects of the TiO_2(B) nanosheet-impregnated HC. The loading rate of the TiO_2(B) into the HC substantially improved the TC removal by the Composite-4 (Table S1).

3.2.2. Effect of pH on TC removal by the composites

In an aqueous solution, pH affects the properties of adsorbate and the surface charge of adsorbate and adsorbent, thereby promoting the columbic forces during adsorption (Zhu et al., 2019). Therefore, the effects of pH on TC removal by the adsorbents were studied.

In order to determine whether pH affects the absorption of UV–vis in TC solution, the UV–vis measurement was used to confirm the maximum

absorbance of TC at pH ranging from 3 to 11. Fig. 5 demonstrates that both acidic and alkaline environment did not have any effects on the UV−vis absorbance properties of TC. This finding was in agreement with those of studies done by Zhou et al. (2019) and Zhang et al. (2019).

Fig. 6a shows that pH 7.0 was optimum for the TC removal by the Composite-1. When the pH increased from 3.0 (pKa_1 of TC) to 7.7 (pKa_2), the TC removal was slightly enhanced from 62% to 78% at 50 mg/L of TC ($p > 0.05$; t-test).

Fig. 6b presents a zeta potential curve of the Composite-1's surfaces at different pH. The zero-point charge of the Composite-1 was at low pH due to the dispersion of the surface charge properties of the colloidal TiO_2 between EG and water during its synthesis (Section 2.2).

The surface of the TiO_2 has several OH^- groups that act as a hole traps to prevent electron-hole recombination (Zhu et al., 2020b). The functional groups contribute their protons to dispersion in water at most pH values. However, as the TiO_2 was immersed in a medium not effective at receiving protons, it was forced to accept protons, leading to positively charged particles. The H_2O addition into the dispersion caused a reduction in the zeta potential of the positively charged TiO_2, getting through an isoelectric point, and then switched the charge to be negative, where the surface of the Composite-1 was expected to be positively charged.

In an acidic pH range, the predominant TC species includes TCH_2, TCH^-, and TCH^{3+} because of dimethyl ammonium group's protonation (Fig. S4), as reported by Ghadim et al. (2013). In the alkaline environment, the zeta potential of the Composite-1 gradually drops and there are repulsive forces between the negatively charged groups of the TC and that of the adsorbent. This leads to a low TC removal by the Composite-1, consistent with the results presented in Fig. 6a.

It is worth noting that once the solution pH changed from 7.7 (pKa_2 of TC) to 11 (pKa_3), the TC removal by the Composite-1 decreased substantially to a negligible level (less than 1%) ($p \leq 0.05$; t-test) because the anionic species (TC_2^- and TCH^-) inhibited TC adsorption due to the adsorbate's less affinity toward the adsorbent's surface (Fig. S4). In an alkaline environment, the predominant TC species includes TCH^- and TC_2^- due to the deprotonations of tricarbonyl as well as phenolic diketone moiety (Duan et al., 2014). A weak π−π electron donor-acceptor interaction between the adsorbate and the surface of the HC might also contribute to a low TC removal at pH 11.

The adsorption mechanisms of the TC by the TiO_2(B)@HC alone (without the addition of H_2O_2) are based on the formation of H-bonding between the adsorbate's molecules and the HC as well as the TiO_2(B) of the TiO_2(B)@HC at pH 5.8 (Fig. S5). Zhu et al. (2013) and Duan et al. (2014) reported that the TC's predominant species is TCH^{3+} present at varying pH between 3.3 and 7.7 and that the $-NH_2$ of the TC molecules is involved in its removal through the carbon surface of the HC via the H-bonding.

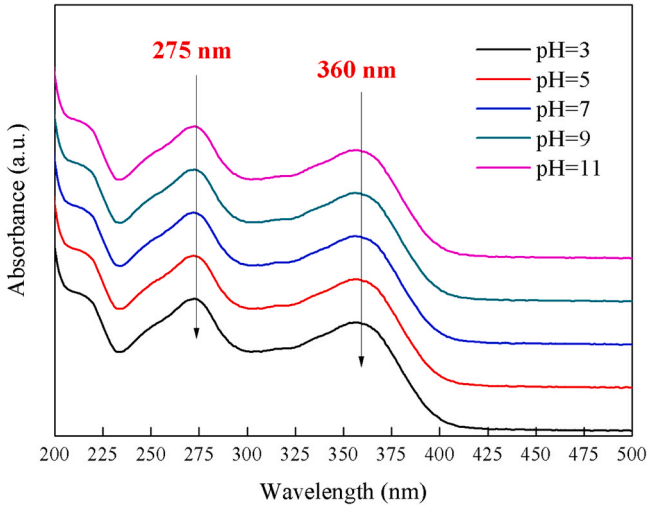

Fig. 5. UV−vis absorbances of TC solution at different pH.

The H-bonding might also contribute to the higher TC removal because of the interactions between the TC molecules and the –OH groups of the TiO_2(B)@HC composite. The formation of H-bonding occurs either (1) between the H-bonds on the surface of the wheat straw (HC) and the aromatic rings of the TC molecules, or (2) the H-bonds of the –OH on the surface of HC or the TiO_2(B) nanosheet (Fig. S5). This adsorption mechanism is in agreement with the result of the study reported by Chen et al. (2017c), who also found the formation of H-bonding between functional groups on the surface of sawdust HC such as C–O, –OH, and –COO– and other functional groups, including C−O and C O.

The oxygen-containing functional groups cause electron transfer via the *Ti–O–C* bond due to their electron affinity. In addition, the surface of the HC has carbon atom with sp^2 bonded structure to delocalize electrons excited from the conduction band (c_b) of the TiO_2(B). Therefore, the composites could suppress electron−hole recombination and delay the recombination time of their electron-hole pairs, thereby maximizing the adsorption process of target pollutant (Kurniawan et al., 2020).

3.3. Kinetic study

3.3.1. TC adsorption kinetics

Fig. S6 depicts the adsorption kinetics of the Composite-1 and the Composite-4 with varying doping of the TiO_2(B) at an initial TC concentration of 10 mg/L. Fig. S6a shows that the rapid removal of the TC by both the composites took place in the first hour, accounting for 83.9% and 84.2%, respectively; then adsorption gradually attained an equilibrium after 4 h, corresponding with 5.1 and 7.5 mg/g of TC adsorption capacities. The adsorption of TC by Composite-4 was slightly faster than that by Composite-1 due to the enlarged surface area in the Composite-4 through increased loading amount of TiO_2(B) nanosheet into the Composite-4 (Table S1).

Without the TiO_2(B) nanosheet, it is interesting to note that the HC alone adsorbed TC so slowly that only about 18% of TC removal was attained (Fig. 4). This indicates that the impregnation of TiO_2(B) nanosheet contributed synergistic effects to both the Composite-1 and the Composite-4 in removing TC more effectively and faster than did the HC alone (Table S3) in terms of TC removal. With respect to the adsorption kinetics, the HC followed the pseudo-second-order model throughout the adsorption reaction.

To evaluate the adsorption of TC onto the Composite-1 and the Composite-4, both the pseudo-first order and the pseudo-second order models were performed to simulate their kinetics data. The intra-particle diffusion of TiO_2(B)@HC controlled the diffusion process of the kinetics (Gupta and Bhattacharyya, 2011). Their fitting curves and other kinetic constants are presented in Fig. S6b and Table S3, respectively.

The coefficient of determination (R^2) is an acceptable way to determine how well fitting curves, as reported by Cao et al. (2018). Table S3 shows that all the R^2 of the above models are greater than 0.94. The coefficient of the pseudo-second order model ($R^2 > 0.997$) was slightly higher than that of the pseudo-first-order ($R^2 > 0.987$). As it is quite difficult to differentiate a certain kinetic model to fit the experimental data, a normalized percent deviation, known as percent relative deviation modulus (P), was introduced to evaluate the performance of the three kinetic models (Ayranci and Duman, 2005).

$$P = \frac{100}{N} \Sigma \frac{\left| C_{t,\mathrm{expt}} - C_{t,pred} \right|}{C_{t,\mathrm{expt}}} \tag{9}$$

where $C_{t,expt}$ is the experimental concentration at any time, $C_{t,pred}$ the corresponding predicted concentration according to the equation under study with best fitted parameters, while N is the number of observations.

The P values were calculated for simulating the kinetic data of the TC adsorption to the three kinetics models (Table S3). The lower the P value

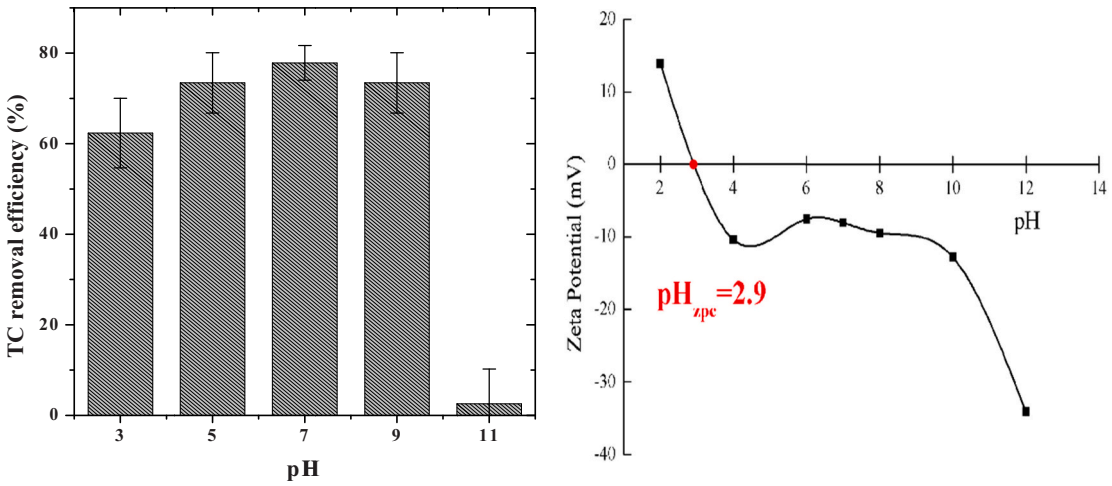

Fig. 6. (a) Effect of pH on TC adsorption by Composite-1. (Optimized conditions: 1 g/L of dose; reaction time: 4 h; TC concentration: 50 mg/L) (b) zeta potential curve of Composite-1 at different equilibrium of pH values.

is, the better the fitness test is, especially when P is less than 5. The linear trends of the plots show that the TC adsorption onto the Composite-4 followed a pseudo-second-order model (Table S3).

In addition, an intra-particle diffusion model was applied to understand the diffusion mechanisms of the TC adsorption by the composite. Fig. S6c presents that the adsorption of TC and the square root of time ($t^{0.5}$) showed a linear relationship ($R^2 > 0.94$), indicating that the intra-particle diffusion mechanisms also played roles in TC removal by the Composite-1 and the Composite-4. This suggests that the TC adsorption by the two composites were due to integrated diffusion-control and surface-control reactions (Rubinstein and Torquato, 1988; Haerifar and Azizian, 2013).

3.3.2. TC adsorption isotherms

Adsorption isotherms studies were conducted to determine the maximum TC adsorption capacity of the HC, the Composite-1 and the Composite-4, respectively, at ambient temperature by varying the TC concentration from 10 to 60 mg/L. Their adsorption isotherms for TC are presented in Fig. S7. It was found that the Freundlich model was more applicable for simulating the isotherm data than the Langmuir isotherm, as reflected by its R^2 and the n_F values (Table S4). This heterogeneous adsorption occurred due to the synergistic effects of the HC and the loaded TiO_2(B) nanosheet into the raw carbon material that has complementary physico-chemical properties to each other.

On the other hand, the maximum TC adsorption capacities of the Composite-1 and the Composite-4 based on the Langmuir model were 40.65 and 49.26 mg/g, respectively (Table S4). This suggests that the loading rate of the TiO_2(B) nanosheet into the HC play roles in enhancing the adsorption capacity of the Composite-4 for the TC.

3.4. Comparison of various low-cost adsorbents for TC removal

Table 1 presents comparative results between this work and previous studies with respect to their optimum conditions such as pH, reaction time, dose and removal efficiencies. The TC adsorption capacity of the Composite-4 was relatively encouraging, as compared to the other adsorbents such as carbon-doped boron nitride (Guo et al., 2020). This finding indicates that the Composite-4 is a promising adsorbent for TC removal from contaminated water.

The TC adsorption capacities of the Composite-4 were higher than those of other materials like chitosan. Kang et al. (2010) reported that a maximum TC adsorption capacity of 41.35 mg/g could be attained by 4 g/L of chitosan with a TC concentration of 470 mg/L. Other adsorbents such as mesoporous BiOI microspheres (Hao et al., 2012), magnetic porous carbon (Zhu et al., 2014) and bamboo charcoal (Liao et al., 2013) achieved a lower TC removal with their concentrations varying from 5 to 100 mg/L, respectively.

With respect to the engineering perspectives of this work for water treatment, theoretically, the TiO_2(B)-based carbon materials such as the Composite-4 may not be practical for industrial scale of water treatment operations, due to their existence in powder form. If it were present in granular, the adsorbent would be practically applicable for a fixed bed column study as long as we take into account varying flow rates, height of the column, mass of the adsorbent in fixed-bed column operations and the characteristics of wastewater effluents to be treated (Kurniawan et al., 2010b, 2012). Lin et al. (2018b) reported that column operations could provide water treatment operators with credible information on acceptable flow rate, breakthrough time, loss of adsorption capacity, and degree of column utilization during consecutive treatment cycles.

Table 1
Comparison of maximum TC adsorption capacity of various low-cost adsorbents for TC removal.

Adsorbents	Max. adsorption capacities (mg/g)	Optimum conditions				References
		Temperature (K)	Dose (g/L)	pH	Initial TC concentration (mg/L)	
Composite-4	49.26	298	1	7	5–100	Present study
Composite-1	40.82	298	1	7	5–100	Present study
Chitosan	41.35	298	4	6.7	1–471	(Kang et al., 2010)
Mesoporous BiOI microspheres	28.35	298	1	NA	NA	(Hao et al., 2012)
Magnetic porous carbon	25.44	303	1	NA	5–80	(Zhu et al., 2014)
Bamboo charcoal	22.70	303	1	7	5–100	(Liao et al., 2013)
Granular sludge	15.22	308	NA	NA	NA	(Shi et al., 2011)
Rice husk ash	8.37	313	2	NA	5–20	(Chen et al., 2016)
Carbon-doped boron nitride	76.74	NA	0.4	7.8	40	(Guo et al., 2020)
Mag-SBE@C	113	NA	2.271	6.5	NA	(Liu et al., 2020)

Remarks: NA: not available

To improve the accuracy of the TC measurement after treatment, instead of UV Vis spectrophotometer, HPLC should be used for pilot scale of this study. The limitations of using the latter instrument include its inability to accurately determine the intermediate products after TC degradation and their possible interference with the adsorption peaks (Su et al., 2021).

3.5. Effect of H_2O_2 addition on TC removal by the composite-1 and composite-4

To enhance the TC removal by the adsorbent, the H_2O_2 was incorporated into the reaction system, which consisted of TiO_2(B) nanosheets and the Composites. Fig. S8 demonstrates the effects of H_2O_2 addition on the TC removal by the two composites.

At the same TC concentration of 50 mg/L, the TC removal by the Composite-1 significantly increased from 45% (before) to 79% (after), while the TC removal by the Composite-4 substantially improved from 64% (before) to 93% (after), when the oxidant's concentration increased to 10 mM.

This indicates that the addition of H_2O_2 during the adsorption reaction resulted in a higher TC removal by the Composite-4 due to oxidative reactions. This also suggests that the TC removal by the TiO_2–functionalized composite after H_2O_2 addition was carried out simultaneously through oxidation and adsorption reactions (Kurniawan and Lo, 2009; Eskelinen et al., 2010; Vilve et al., 2010; Sillanpaa et al., 2011). Through oxidation processes (Reaction 10–14), the target pollutant was degraded into smaller and more biodegradable oxidation by-products. The remaining by-products were further removed by the composites through adsorption processes.

Initiation.

$$H_2O_2 + HO^- \rightarrow HO_2^- + H_2O \quad (10)$$

$$HC^+ + H_2O_2 \rightarrow HC + H^+ + HO_2\cdot \quad (11)$$

Propagation.

$$HO_2\cdot \rightarrow H^+ + \cdot O_2^- \; pKa = 4{\cdot}8 \quad (12)$$

$$\cdot O_2^- + H_2O_2 \rightarrow \cdot OH + OH^- + O_2 \quad (13)$$

Termination.

$$\cdot OH + \text{target pollutant} \rightarrow \text{oxidation by-products} \; k = 1{\cdot}6 \times 10^9 \; M^{-1} \; s^{-1} \quad (14)$$

In the absence of carbon-rich composite in control experiments (Fig. S7), Chen et al. (2017a) reported that TC removal took place due to a direct molecular reaction with the oxidant, instead of active species such as $\cdot O_2^-$/ $HO_2\cdot$. This finding was in agreement with that of previous study carried out by Kurniawan and Lo (2009), who found that an integrated treatment of activated carbon adsorption and H_2O_2 resulted in the generation of active species that degraded refractory compounds in the samples of stabilized leachate. This suggests that the hydrochar (HC) alone might be responsible for the H_2O_2 decomposition that led to the TC degradation in the samples.

3.6. Regeneration of TiO_2(B)@HCs

To prevent the undesirable transfer of pollutants from aqueous solutions into another medium after treatment and to sustain their life time for cost-effectiveness, the spent adsorbents were regenerated and reused after it became saturated with TC. In this study, the reusability of the Composite-1 was tested by adsorption using 0.1 M NaOH.

Table S5 shows the recovery rate of TC from the exhausted Composite-1 and Composite-4 after their first regeneration. About 86% and 89.4% of TC recovery (5.47 mg/g and 7.92 mg/g of TC adsorption capacities, respectively) were attained by Composite-1 and Composite-4, respectively. This suggests that the Composite-1 and the Composite-4 can be used in subsequent cycle for TC removal. However, after second cycle of their regeneration, the regeneration efficiencies of both composites were very low (less than 50%). Although their crystal structure, morphology, and surface were not destroyed during the regeneration, the adsorbed TC could not be completely desorbed by the adsorbents because regeneration of the adsorbent involved only physico-chemical processes.

Practically, it is not feasible to retain the reusability of the spent composites after the second cycle of their regeneration. This represents a common drawback of saturated adsorbents in water treatment applications. To mitigate this bottleneck, calcination may be able to recycle the same composites after being saturated without affecting their original properties with respect to selectivity and/or capacity toward the target pollutant in subsequent treatment. Overall, this result implies the reusability of the spent composites for TC removal from aqueous solution by adsorption processes.

4. Conclusions

We have demonstrated the performance of the TiO_2(B)@carbon composites (Composite-1, Composite-2, Composite-3, and Composite-4) for TC removal from wastewater. It was evident that under optimized conditions (pH 7, initial TC concentration of 50 mg/L, 1 g/L of absorbent dose, and 4 h of reaction time), the Composite-1 had the highest TC removal (46%), as compared to the Composite-2 (38%) and the Composite-3 (35%). The TC adsorption capacities of the Composite-1 and the Composite-4 were 40.65 and 49.26 mg/g, respectively. The addition of H_2O_2 (10 mM) enhanced the TC removal by the Composite-1 and the Composite-4 from 45% to 79%, and from 64% to 93%, respectively. The TC removal by the Composite-1 followed the pseudo-second order model. Overall, this work suggests that converting the wheat straw waste into HC and then functionalizing its surface with the TiO_2(B) nanosheets as a composite has added technological values to the unused resources and that the product was promising for TC removal after its surface modification.

CRediT authorship contribution statement

Zhu Mengting is responsible for overall Investigation and data collection. Tonni Agustiono Kurniawan is responsible for project Supervision, re-writing original draft; Writing - review & editing; Funding acquisition. Huang Yujia and Zhang Xueting are responsible for data analysis. Tong Ouyang, Iswanto, Tjandra Setiadi are responsible for Resources and Project administration. Mohd. Hafiz Dzarfan Othman and Ram Avtar are responsible for Conceptualization and Validation.

Declaration of Competing Interest

The authors declare that they have no known competing financial interests or personal relationships that could have appeared to influence the work reported in this paper.

Acknowledgements

The corresponding author is grateful to the TWAS–Elsevier Foundation and the TYAN of the World Academy of Sciences, respectively, for the Fellowship in Sustainability No. FR 3240292438 and the Collaborative Grant Award No. FR 3240304540. The Fellowship from the TWAS–UNESCO Associateship No. 3240314536 is also acknowledged. This research was also supported in part with the Kurita Asia Research Grant provided by the Kurita Water and Environment Foundation (Japan).

Appendix A. Supporting information

Supplementary data associated with this article can be found in the online version at doi:10.1016/j.jhazmat.2020.123999.

References

Ahmad, M., Rajapaksha, A.U., Lim, J.E., Zhang, M., Bolan, N., Mohan, D., Vithanage, M., Lee, S.S., Ok, Y.S., 2014. Biochar as a sorbent for contaminant management in soil and water: a review. Chemosphere 99, 19–33. https://doi.org/10.1016/j.chemosphere.2013.10.071.

Albadarin, A.B., Solomo, S., Kurniawan, T.A., Mangwandi, C., Walker, G., 2017. Single, simultaneous and consecutive biosorption of Cr(VI) and orange II onto chemically modified masau stones. J. Environ. Manag. 204, 365–374. https://doi.org/10.1016/j.jenvman.2017.08.042.

Ayranci, E., Duman, O., 2005. Adsorption behaviors of some phenolic compounds onto high specific area activated carbon cloth. J. Hazard. Mater. 124, 125–132. https://doi.org/10.1016/j.jhazmat.2005.04.020.

Babel, S., Kurniawan, T.A., 2003. Low-cost adsorbents for heavy metals uptake from contaminated water: a review. J. Hazard. Mater. 97, 219–243. https://doi.org/10.1016/S0304-3894(02)00263-7.

Babel, S., Kurniawan, T.A., 2004. Cr(VI) removal from synthetic wastewater using coconut shell charcoal and commercial activated carbon modified with oxidizing agents and/or chitosan. Chemosphere 54, 951–967. https://doi.org/10.1016/j.chemosphere.2003.10.001.

Cao, J., Yang, Z.H., Xiong, W.P., Zhou, Y.Y., Peng, Y.R., Li, X., Zhou, C.Y., Xu, R., Zhang, Y.R., 2018. One-step synthesis of Co-doped UiO-66 nanoparticle with enhanced removal efficiency of tetracycline: simultaneous adsorption and photocatalysis. Chem. Eng. J. 353, 126–137. https://doi.org/10.1016/j.cej.2018.07.060.

Chan, G., Chang, J., Kurniawan, T.A., Fu, C.X., Jiang, H., Je, Y., 2007. Removal of non-biodegradable compounds from stabilized leachate using VSEPRO membrane filtration. Desalination 202, 310–317. https://doi.org/10.1016/j.desal.2005.12.069.

Chen, S.Q., Chen, Y.L., Jiang, H., 2017a. Slow pyrolysis magnetization of hydrochar for effective and highly stable removal of tetracycline from aqueous solution. Ind. Eng. Chem. Res. 56, 3059–3066. https://doi.org/10.1021/acs.iecr.6b04683.

Chen, W., Wei, L., Lin, Z., Liu, Q., Chen, Y., Lin, Y., Huang, Z., 2017b. Hierarchical flower-like $NiCo_2O_4$@TiO_2 hetero-nanosheets as anodes for lithium ion batteries. RSC Adv 7, 47602–47613. https://doi.org/10.1039/C7RA09024B.

Chen, Y.Y., Ma, Y.L., Yang, J., Wang, L.Q., Lv, J.M., Ren, C.J., 2017c. Aqueous tetracycline degradation by H_2O_2 alone: removal and transformation pathway. Chem. Eng. J. 307, 15–23. https://doi.org/10.1016/j.cej.2016.08.046.

Chen, Y.J., Wang, F.H., Duan, L.C., Yang, H., Gao, J., 2016. Tetracycline adsorption onto rice husk ash, an agricultural waste: its kinetic and thermodynamic studies. J. Mol. Liq. 222, 487–494. https://doi.org/10.1016/j.molliq.2016.07.090.

Donar, Y.O., Bilge, S., Sınağ, A., Pliekhov, O., 2018. TiO_2/carbon materials derived from hydrothermal carbonization of waste biomass: a highly efficient, low-cost visible-light-driven photocatalyst. ChemCatChem 10, 1134–1139. https://doi.org/10.1002/cctc.201701405.

Duan, L., Li, L., Xu, Z., Chen, W., 2014. Adsorption of tetracycline to nano-NiO: the effect of co-existing Cu(II) ions and environmental implications. Environ. Sci. Process. Impacts 16, 1462–1468. https://doi.org/10.1039/C4EM00096J.

Eskelinen, K., Sarkka, H., Kurniawan, T.A., Sillanpaa, M., 2010. Removal of recalcitrant contaminants from bleaching effluents in pulp and paper mills using ultrasonic irradiation and Fenton-like oxidation, electrochemical treatment, and/or chemical precipitation: a comparative study. Desalination 255, 179–187. https://doi.org/10.1016/j.desal.2009.12.024.

Fu, D., Huang, Y.J., Zhang, X.T., Kurniawan, T.A., Ouyang, T., 2017. Uncovering potentials of integrated TiO_2(B) nanosheets and H_2O_2 for removal of tetracycline from aqueous solution. J. Mol. Liq. 248, 112–120. https://doi.org/10.1016/j.molliq.2017.10.020.

Garlapalli, R.K., Wirth, B., Reza, M.T., 2016. Pyrolysis of hydrochar from digestate: effect of hydrothermal carbonization and pyrolysis temperatures on pyrochar formation. Biores. Technol. 220, 168–174. https://doi.org/10.1016/j.biortech.2016.08.071.

Gerasimova, T.V., Evdokimova, O.L., Kraev, A.S., Ivanov, V.K., Agafonov, A.V., 2016. Micro-mesoporous anatase TiO_2 nanorods with high specific surface area possessing enhanced adsorption ability and photocatalytic activity. Microporous Mesoporous Mater. 235, 185–194. https://doi.org/10.1016/j.micromeso.2016.08.015.

Ghadim, E.E., Manouchehri, F., Soleimani, G., Hosseini, H., Kimiagar, S., Nafisi, S., 2013. Adsorption properties of tetracycline onto graphene oxide: equilibrium, kinetic and thermodynamic studies. PLOS One 8, e79254. https://doi.org/10.1371/journal.pone.0079254.

Guo, Y., Yan, C.C., Wang, P.F., Rao, L., Wang, C., 2020. Doping of carbon into boron nitride to get the increased adsorption ability for tetracycline from water by changing the pH of solution. Chem. Eng. J. 387, 124136 https://doi.org/10.1016/j.cej.2020.124136.

Gupta, S.S., Bhattacharyya, K.G., 2011. Kinetics of adsorption of metal ions on inorganic materials: a review. Adv. Colloid Int. Sci. 162, 39–58. https://doi.org/10.1016/j.cis.2010.12.004.

Haerifar, M., Azizian, S., 2013. Mixed surface reaction and diffusion-controlled kinetic model for adsorption at the solid/solution interface. J. Phys. Chem. C 117, 8310–8317. https://doi.org/10.1021/jp401571m.

Han, M.J., Jiang, K.K., Jiao, P.F., Ji, Y.C., Zhou, J.W., Zhuang, W., Chen, Y., Liu, D., Zhu, C.J., Chen, X.C., Ying, H.J., Wu, J.L., 2017. Bio-butanol sorption performance on novel porous-carbon adsorbents from corncob prepared via hydrothermal carbonization and post-pyrolysis method. Sci. Rep. 7, 1–11. https://doi.org/10.1038/s41598-017-12062-7.

Hao, R., Xiao, X., Zuo, X.X., Nan, J.M., Zhang, W.D., 2012. Efficient adsorption and visible-light photocatalytic degradation of tetracycline hydrochloride using mesoporous BiOI microspheres. J. Hazard. Mater. 209, 137–145. https://doi.org/10.1016/j.jhazmat.2012.01.006.

Kambo, H.S., Dutta, A., 2015. A comparative review of biochar and hydrochar in terms of production, physico-chemical properties and applications. Renew. Sustain. Energy Rev. 45, 359–378. https://doi.org/10.1016/j.rser.2015.01.050.

Kang, J., Liu, H.J., Zheng, Y.M., Qu, J.H., Chen, J.P., 2010. Systematic study of synergistic and antagonistic effects on adsorption of tetracycline and copper onto a chitosan. J. Colloid Interface Sci. 344, 117–125. https://doi.org/10.1016/j.jcis.2009.11.049.

Kearns, J.P., Wellborn, L.S., Summers, R.S., Knappe, D.R.U., 2014. 2,4-D adsorption to biochars: effect of preparation conditions on equilibrium adsorption capacity and comparison with commercial activated carbon literature data. Water Res. 62, 20–28. https://doi.org/10.1016/j.watres.2014.05.023.

Kommireddy, D.S., Sriram, S.M., Lvov, Y.M., Mills, D.K., 2006. Stem cell attachment to layer-by-layer assembled TiO_2 nanoparticle thin films. Biomaters 27, 4296–4303. https://doi.org/10.1016/j.biomaterials.2006.03.042.

Kong, X.C., Xu, Y., Cui, Z.D., Li, Z.Y., Liang, Y.Q., Gao, Z.H., Zhu, S.L., Yang, X.J., 2018. Defect enhances photocatalytic activity of ultrathin TiO_2(B) nanosheets for hydrogen production by plasma engraving method. Appl. Catal. B Environ. 230, 11–17. https://doi.org/10.1016/j.apcatb.2018.02.019.

Kumar, P.S., Korving, L., Keesman, K.J., Loosdrecht, M.C.M., Witkamp, G.J., 2019. Effect of pore size distribution and particle size of porous metal oxides on phosphate adsorption capacity and kinetics. Chem. Eng. J. 358, 160–169. https://doi.org/10.1016/j.cej.2018.09.202.

Kurniawan, T.A., Lo, W.H., Chan, G., 2006a. Degradation of recalcitrant compounds from stabilized landfill leachate using a combination of ozone-GAC adsorption treatment. J. Hazard. Mater. 137, 443–455. https://doi.org/10.1016/j.jhazmat.2006.02.020.

Kurniawan, T.A., Lo, W.H., Chan, G., 2006b. Radicals-catalyzed oxidation reactions for degradation of recalcitrant compounds from landfill leachate. Chem. Eng. J. 125, 35–57. https://doi.org/10.1016/j.cej.2006.07.006.

Kurniawan, T.A., Chan, G., Lo, W.H., Babel, S., 2006c. Comparison of low-cost adsorbents for treating wastewaters laden with heavy metals. Sci. Total Environ. 366, 409–426. https://doi.org/10.1016/j.scitotenv.2005.10.001.

Kurniawan, T.A., Chan, G., Lo, W.H., Babel, S., 2006d. Physico-chemical treatment techniques for wastewater laden with heavy metal. Chem. Eng. J. 118, 83–98. https://doi.org/10.1016/j.jhazmat.2005.08.010.

Kurniawan, T.A., Lin, Y.Y., Ouyang, T., Albadarin, A.B., Walker, G., 2018. $BaTiO_3$/TiO_2 composite-assisted photocatalytic degradation for removal of acetaminophen from synthetic wastewater under UV–VIS irradiation. Mater. Sci. Semicond. Process. 73, 42–50. https://doi.org/10.1016/j.mssp.2017.06.048.

Kurniawan, T.A., Lo, W.H., 2009. Removal of refractory compounds from stabilized landfill leachate using an integrated H_2O_2 oxidation and granular activated carbon (GAC) adsorption treatment. Water Res 43, 4079–4091. https://doi.org/10.1016/j.watres.2009.06.060.

Kurniawan, T.A., Lo, W.H., Chan, G., Sillanpaa, M., 2010b. Biological processes for treatment of landfill leachate. J. Environ. Monit. 12, 2032–2047. https://doi.org/10.1039/c0em00076k.

Kurniawan, T.A., Lo, W.H., Sillanpaa, M., 2011. Treatment of contaminated water laden with 4-chlorophenol using coconut shell waste-based activated carbon modified with chemical agents. Sep. Sci. Technol. 46, 460–472. https://doi.org/10.1080/01496395.2010.512030.

Kurniawan, T.A., Oliveira, J.P., Gamaralalage, P.J.D., Nagaishi, M., 2013. City-to-city level cooperation for generating urban co-benefits: the case of technological cooperation in the waste sector between Surabaya (Indonesia) and Kitakyushu (Japan). J. Cleaner Prod. 58, 43–50. https://doi.org/10.1016/j.jclepro.2013.08.002.

Kurniawan, T.A., Sillanpaa, M., Sillanpaa, M., 2012. Nanoadsorbents for remediation of aquatic environment: local and practical solutions for global pollution problems. Crit. Rev. Environ. Sci. Technol. 42, 1233–1295. https://doi.org/10.1080/10643389.2011.556553.

Kurniawan, T.A., Waihung, L., Repo, E., Sillanpaa, M., 2010a. Removal of 4-chlorophenol from contaminated water using coconut shell waste pretreated with chemical agents. J. Chem. Technol. Biotechnol. 85, 1616–1627. https://doi.org/10.1002/jctb.2473.

Kurniawan, T.A., Zhu, M.T., Fu, D., Keong, Y.S., Othman, M.H.D., Avtar, R., Hwang, G.H., 2020. Functionalizing TiO_2 with graphene oxide for enhancing photocatalytic degradation of methylene blue (MB) in contaminated wastewater. J. Environ. Manag. 270, 110871 https://doi.org/10.1016/j.jenvman.2020.110871.

Lehmann, J., Joseph, S., 2015. Biochar for environmental management: an introduction. In: Lehman, S., Joseph, S. (Eds.), Biochar for Environmental Management: Science, Technology and Implementation. Routledge, New York, pp. 1–12. https://doi.org/10.4324/9780203762264.

Liao, P., Zhan, Z.Y., Dai, J., Wu, X.H., Zhang, W.B., Wang, K., Yuan, S.H., 2013. Adsorption of tetracycline and chloramphenicol in aqueous solutions by bamboo charcoal: a batch and fixed-bed column study. Chem. Eng. J. 228, 496–505. https://doi.org/10.1016/j.cej.2013.04.118.

Lin, Y.Y., Kurniawan, T.A., Albadarin, A.B., Walker, G., 2018a. Enhanced removal of acetaminophen from synthetic wastewater using multi-walled carbon nanotubes (MWCNT) chemically modified with NaOH, HNO_3/H_2SO_4, ozone, and/or chitosan. J. Mol. Liq. 251, 369–377. https://doi.org/10.1016/j.mssp.2017.06.048.

Lin, Y.Y., Kurniawan, T.A., Zhu, M.T., Ouyang, T., Avtar, R., Othman, M.H.D., Mohammad, B.T., Albadarin, A.B., 2018b. Removal of acetaminophen from synthetic wastewater in a fixed-bed column adsorption using low-cost coconut shell waste pretreated with NaOH, HNO_3, ozone, and/or chitosan. J. Environ. Manag. 226, 365–376. https://doi.org/10.1016/j.jenvman.2018.08.032.

Lin, Y.Y., Kurniawan, T.A., Ying, Z., Albadarin, A.B., Walker, G., 2017. Enhanced photocatalytic degradation of acetaminophen from wastewater using WO_3/TiO_2/SiO_2 composite under UV–VIS irradiation. J. Mol. Liq. 243, 761–770. https://doi.org/10.1016/j.molliq.2017.08.092.

Lisowski, P., Colmenares, J.C., Masek, O., Lisowski, W., Lisovytskiy, D., Kaminska, A., Lomot, D., 2017. Dual functionality of TiO_2/biochar hybrid materials: photocatalytic phenol degradation in the liquid phase and selective oxidation of methanol in the gas phase. ACS Sustain. Chem. Eng. 5, 6274–6287. https://doi.org/10.1021/acssuschemeng.7b01251.

Liu, Y.D., Li, J.S., Wu, L.R., Shi, Y.H., He, Q.C., Chen, J., Wan, D.J., 2020. Magnetic spent bleaching earth carbon (Mag-SBE@C) for efficient adsorption of tetracycline hydrochloride: response surface methodology for optimization and mechanism of action. Sci. Total Environ. 722, 137817 https://doi.org/10.1016/j.scitotenv.2020.137817.

Liu, X.H., Lu, S.Y., Meng, W., Wang, W.L., 2018. Occurrence, source, and ecological risk of antibiotics in Dongting Lake, China. Environ. Sci. Pollut. Res. 25, 11063–11073. https://doi.org/10.1007/s11356-018-1290-1.

Li, X.M., Shen, Q.R., Zhang, D.Q., Mei, X.L., Ran, W., Xu, Y.C., Yu, G.H., 2013. Functional groups determine biochar properties (pH and EC) as studied by two-dimensional ^{13}C NMR correlation spectroscopy. PLOS One 8, e65949. https://doi.org/10.1371/journal.pone.0065949.

Mangwandi, C., Kurniawan, T.A., Albadarin, A.B., 2020. Comparative biosorption of chromium (VI) using chemically modified date pits (CM-DP) and olive stone (CM-OS): kinetics, isotherms and influence of co-existing ions. Chem. Eng. Res. Des. 156, 251–262. https://doi.org/10.1016/j.cherd.2020.01.034.

Meyer, S., Glaser, B., Quicker, P., 2011. Technical, economical, and climate-related aspects of biochar production technologies: a literature review. Environ. Sci. Technol. 45, 9473–9483. https://doi.org/10.1021/es201792c.

Nadeem, I.M., Harrison, G.T., Wilson, A., Pang, C.L., Zegenhagen, J., Thorntonei, G., 2018. Bridging hydroxyls on anatase TiO_2(101) by water dissociation in oxygen vacancies. J. Phys. Chem. B 122, 834–839. https://doi.org/10.1021/acs.jpcb.7b06955.

Narzari, R., Bordoloi, N., Chutia, R.S., Borkotoki, B., Gogoi, N., Bora, A., Kataki, R., 2014. Biochar: an overview on its production, properties and potential benefits. In: Choudhuri, H. (Ed.), Biology, Biotechnology and Sustainable Development. Res. India Public, New Delhi, pp. 13–40. https://doi.org/10.13140/RG.2.1.3966.2560.

Rubinstein, J., Torquato, S., 1988. Diffusion-controlled reactions: mathematical formulation, variational principles, and rigorous bounds. J. Chem. Phys. 88, 6372–6380. https://doi.org/10.1063/1.454474.

Shi, Y.J., Wang, X.H., Qi, Z., Diao, M.H., Gao, M.M., Xing, S.F., Wang, S.G., Zhao, X.C., 2011. Sorption and biodegradation of tetracycline by nitrifying granules and the toxicity of tetracycline on granules. J. Hazard. Mater. 191, 103–109. https://doi.org/10.1016/j.jhazmat.2011.04.048.

Sillanpaa, M., Kurniawan, T.A., Lo, W.H., 2011. Degradation of chelating agents in aqueous solution using advanced oxidation process (AOP). Chemosphere 83, 1443–1460. https://doi.org/10.1016/j.chemosphere.2011.01.007.

Su, Y.P., Li, S., Jiang, G., Zheng, Z., Wang, C., Zhao, S., Cui, D., Liu, Y., Zhang, B., Zhang, Z., 2021. Synergic removal of tetracycline using hydrophilic three-dimensional nitrogen-doped porous carbon embedded with copper oxide nanoparticles by coupling adsorption and photocatalytic oxidation processes. J. Colloid Interface Sci. 581, 350–361. https://doi.org/10.1016/j.jcis.2020.07.071.

Vilve, M., Vilhunen, S., Vepsäläinen, M., Kurniawan, T.A., Lehtonen, N., Isomäki, H., Sillanpää, M., 2010. Degradation of 1,2-dichloroethane from contaminated water laden with ion-exchange resin using Fenton oxidation. Environ. Sci. Pollut. Res. 17, 875–884. https://doi.org/10.1007/s11356-009-0291-5.

Woolf, D., James, E., Amonette, F., Street-Perrott, A., Lehmann, J., Stephen, J., 2010. Sustainable biochar to mitigate global climate change. Nat. Commun. 1, 1–9. https://doi.org/10.1038/ncomms1053.

Xiang, G.L., Li, T.Y., Zhuang, J., Wang, X., 2010. Large-scale synthesis of metastable TiO_2(B) nanosheets with atomic thickness and their photocatalytic properties. Chem. Commun. 46, 6801–6803. https://doi.org/10.1039/C0CC02327B.

Xue, Y.W., Gao, B., Yao, Y., Inyang, M., Zhang, M., Zimmerman, A.R., Ro, K.S., 2012. Hydrogen peroxide modification enhances the ability of biochar (hydrochar) produced from hydro-thermal carbonization of peanut hull to remove aqueous heavy metals: batch and column tests. Chem. Eng. J. 200, 673–680. https://doi.org/10.1016/j.cej.2012.06.116.

Yao, M., Ji, Y., Wang, H., Ao, Z., Li, G., An, T., 2017. Adsorption mechanisms of typical carbonyl-containing volatile organic compounds on anatase TiO_2 (001) surface: a DFT investigation. J. Phys. Chem. C 121, 13717–13722. https://doi.org/10.1021/acs.jpcc.7b02964.

Yusof, M.S.M., Othman, M.H.D., Wahab, R.A., Jumbri, K., Razak, F.I.A., Kurniawan, T.A., Samah, R.A., Mustafa, A., Rahman, M.A., Jaafar, J., Ismail, A.F., 2020a. Arsenic adsorption mechanism on palm oil fuel ash (POFA) powder suspension. J. Hazard. Mater. 383, 121214 https://doi.org/10.1016/j.jhazmat.2019.121214.

Yusof, M.S.M., Othman, M.H.D., Wahab, R.A., Samah, Kurniawan, T.A., Mustafa, A., Rahman, M.A., Jaafar, J., Ismail, A.F., 2020b. Effects of pre and post-ozonation on POFA hollow fibre ceramic adsorptive membrane for arsenic removal in water. J. Taiwan Inst. Chem. Eng. 110, 100–111. https://doi.org/10.1016/j.jtice.2020.02.014.

Zhang, P.Z., Li, Y.F., Cao, Y.Y., Han, L.J., 2019. Characteristics of tetracycline adsorption by cow manure biochar prepared at different pyrolysis temperatures. Biores. Technol. 285, 121348 https://doi.org/10.1016/j.biortech.2019.121348.

Zhang, Q.Q., Ying, G.G., Pan, C.G., Liu, Y.S., Zhao, J.L., 2015. Comprehensive evaluation of antibiotics emission and fate in the river basins of China: source analysis, multimedia modeling, and linkage to bacterial resistance. Environ. Sci. Technol. 49, 6772–6782. https://doi.org/10.1021/acs.est.5b00729.

Zhou, Y.Y., He, Y.Z., He, Y.Z., Liu, X.C., Xu, B., Yu, J.F., Dai, C.H., Huang, A.Q., Pang, Y., Luo, L., 2019. Analyses of tetracycline adsorption on alkali-acid modified magnetic biochar: site energy distribution consideration. Sci. Total Environ. 650, 2260–2266. https://doi.org/10.1016/j.scitotenv. 2018.09.393.

Zhu, M.T., Kurniawan, T.A., Song, F., Ouyang, T., Othman, M.H.D., Rezakazemi, M., Shirazian, S., 2019. Applicability of $BaTiO_3$/graphene oxide (GO) composite for enhanced photodegradation of methylene blue (MB) in synthetic wastewater under UV–vis irradiation. Environ. Pollut. 255, 113182 https://doi.org/10.1016/j.envpol.2019.113182.

Zhu, M.T., Kurniawan, T.A., You, Y., Othman, M.H.D., Avtar, R., 2020a. 2D Graphene oxide (GO) doped p-n type BiOI/Bi2WO6 as a novel composite for photodegradation of bisphenol A (BPA) in aqueous solutions under UV vis irradiation. Mater. Sci. Eng. C 108, 110420. https://doi.org/10.1016/j.msec.2019.110420.

Zhu, M.T., Kurniawan, T.A., You, Y.P., Othman, M.H.D., Avtar, R., Fu, D., Hwang, G.H., 2020b. Fabrication, characterization, and application of ternary magnetic recyclable Bi_2WO_6/ BiOI@Fe_3O_4 composite for photodegradation of tetracycline in aqueous solution. J. Environ. Manag. 270, 110839 https://doi.org/10.1016/j.jenvman.2020.110839.

Zhu, X.D., Liu, Y.C., Qian, F., Zhou, C., Zhang, S.C., Chen, J.M., 2014. Preparation of magnetic porous carbon from waste hydrochar by simultaneous activation and magnetization for tetracycline removal. Biores. Technol. 154, 209–214. https://doi.org/10.1016/j.biortech.2013.12.019.

Zhu, X.D., Wang, Y.J., Sun, R.J., Zhou, D.M., 2013. Photocatalytic degradation of tetracycline in aqueous solution by nanosized TiO_2. Chemosphere 92, 925–932. https://doi.org/10.1016/j.chemosphere. 2013.02.066.